J Solid State Electrochem (2012) 16:1761–1766
DOI 10.1007/s10008-011-1592-4

ORIGINAL PAPER

Crystalline phase content and ionic conductivity correlation in LATP glass–ceramic

Swati Soman · Yoshiki Iwai · Junichi Kawamura · Ajit Kulkarni

Received: 29 August 2011 / Revised: 6 October 2011 / Accepted: 8 November 2011 / Published online: 22 November 2011

Abstract Li_2O–Al_2O_3–TiO_2–P_2O_5 (LATP) glass was fabricated by conventional melt quenching route. Glass transition temperature (T_g=296 °C) and crystallization temperatures ($T_{C1,2}$) were obtained from thermal analysis. LATP glass was converted to glass–ceramic by heat treatment in the range 550–950 °C for 6 h. X-ray diffraction analysis revealed $LiTi_2(PO_4)_3$ as a major phase. Ionic conductivity increased monotonically with concentration, reaching a maximum of ~10^{-4} S/cm. $AlPO_4$ phase was detected in samples heat-treated above 850 °C. Its presence decreased the conductivity, suggesting $LiTi_2(PO_4)_3$ phase as main contributor to high ionic conductivity. NMR spectra confirmed the presence of mobile ^7Li ions in the entire sample series and also gave some information on the structure and dynamics of conductivity.

Keywords LATP glass · Glass–ceramic · Electrical conductivity · Solid electrolytes

Introduction

Lithium ion microbatteries for present miniature and future nano devices are the recent focus in battery research. Microbatteries fabricated using pulse laser deposition techniques are reported in the literature [1–4]. Thin solid films are used as electrolytes in these all-solid-state batteries. The thin electrolytes should be continuous without any pin holes, besides possessing high ionic conductivity in operational temperature range. Dense glass–ceramic materials become suitable candidates for such purpose.

One such class of materials is based on $LiTi_2(PO_4)_3$ (LTP) and compounds derived from it by partial substitution of Ti with Al, Ge, Sc, In, Zr, Hf, etc. [5, 6]. Significant improvement in conductivity is reported when Al is substituted into the parent LTP lattice. Different stoichiometries of LATP are studied [7–9]. However, pellet pressing followed by sintering always yields finite amount of porosity [6].

To overcome this limitation, we followed melt quenching approach for fabrication of LATP, as described by Fu, and converted the glassy form of LATP into glass–ceramic by heat treatment [10]. In this paper, we compare our results with those reported earlier on similarly processed samples as well as samples fabricated by pellet pressing and sintering method [10–13].

Experimental details

Glass was fabricated using conventional melt quenching technique. Laboratory reagent-grade chemicals Li_2CO_3, $NH_4H_2PO_4$, $Al(OH)_3$, and TiO_2, used as starting materials, were mixed thoroughly in appropriate molar ratio to fabricate 50 g of $14Li_2O$–$9Al_2O_3$–$38TiO_2$–$39P_2O_5$ glass. The batch was initially heated to 700 °C for 1 h in Pt crucible to release volatile products of the reaction and subsequently melted at 1,450 °C for 2 h. The homogeneous melt was

S. Soman (✉) · A. Kulkarni (✉)
Department of Metallurgical Engineering and Materials Science,
Indian Institute of Technology Bombay,
Mumbai 400076, India
e-mail: somans@iitb.ac.in
e-mail: ajit.kulkarni@iitb.ac.in

Y. Iwai · J. Kawamura
Institute of Multidisciplinary Research for Advanced Materials
(IMRAM), Tohoku University,
Katahira 2-1-1, Aobaku,
Sendai 980-8577, Japan

quenched between preheated brass plates (~ 300 °C). The glass thus formed was cooled very slowly to room temperature.

T_g and crystallization temperatures were determined using Differential Thermal Analysis (QA Instruments) at a heating rate of 5 K/min.

LATP glass was heat treated at 550 °C, which is slightly above T_{c1} (= 536 °C) for different time durations of 6 h, 12 h and 24 h. These samples showed almost the same values of their dc ionic conductivity. Further, heat treatment was carried out in the temperature range 550–950 °C, i.e., above first crystallization temperature and below melting point, for 6 h each.

Powder X-ray diffraction (XRD) was recorded on Philips Xpert PRO diffractometer using Cu-Kα line (1.54 Å) at room temperature. Crystalline phases were identified by comparing the observed data with the standards from International Centre for Diffraction Data.

NMR measurements were performed on Bruker Avance 600 spectrometer with a magnetic field of 14.1 T. ^{7}Li NMR measurements were performed at 233 MHz (with a reference of LiCl aqueous solution). Spectra were recorded using an excitation pulse of 90° with pulse length of 6 µs. Eight scans were used. ^{27}Al was measured at 156 MHz (α Al_2O_3 powder used as reference) with 128 or 512 scans and 90° pulse length of 1 µs. MAS NMR measurements were performed at a spinning speed of 20 kHz.

^{31}P was measured at 243 MHz using $NH_4H_2PO_4$ powder as standard. A total of 16 scans were recorded with 90° pulse length of 2 µs. MAS NMR measurements were performed at a spinning speed of 10 kHz.

Conductivity measurements were carried out by impedance spectroscopy method using Solatron 1260 with 1296 interface impedance analyzer. Samples were cut and polished to obtain uniform thickness and flat surfaces. Opposite faces were coated with Ag paint for good electrical contact. Ag paint was dried at room temperature in dry atmosphere for several hours. Good electrical continuity of the coated surfaces was ensured before loading the samples in a setup for conductivity measurements. The impedance data were acquired over 10 mHz–1 MHz in the temperature range −50 to 300 °C. DC resistance at each temperature was obtained from intercept on the real axis (impedance plot) and was used to calculate dc conductivity.

Results and discussion

Thermal analysis

The first characterization of as-cast glass was done by thermal analysis. T_g from DTA measurement was estimated to be 296 °C. Two crystallization temperatures were also identified at 536 and 635 °C, respectively. No melting was observed up to 1,000 °C.

X ray diffraction measurements

Figure 1 shows the XRD patterns of a few glass–ceramic samples obtained by heat treatment at different temperatures for 6 h. XRD pattern of the as-cast glass is included for comparison. It showed a broad feature without any distinct peaks, confirming the amorphous nature of the glass. Diffraction peaks arising from $LiTi_2(PO_4)_3$ were observed in all glass–ceramic samples, indicating $LiTi_2(PO_4)_3$ as a major crystalline phase present above the first crystallization temperature (~ 536 °C). The intensity of these peaks increased with the heat treatment temperature, implying that $LiTi_2(PO_4)_3$ phase grew gradually with temperature. At 900 °C and above, diffraction peaks corresponding to $AlPO_4$ phase could also be identified. $AlPO_4$ nanocrystals started to precipitate above the second crystallization temperature. At higher temperatures, their peak intensity became appreciable. The diffraction peak positions were matched with the JCPDS standards and the lattice constants were found. $LiTi_2(PO_4)_3$ was rhombohedral with a=8.512 Å and c=20.878 Å. $AlPO_4$ was triclinic with a=13.46 Å, b=22.17 Å, c=5.29 Å and α=90.16°, β= 92.01°, γ=89.95°.

Impedance spectroscopic measurements

Figure 2a shows the complex impedance plot for as-cast glass sample. A curvature observed in the high frequency range was fitted to the impedance response of an RC parallel circuit. The value of R was obtained from the intercept of the semicircle on real axis and C was calculated

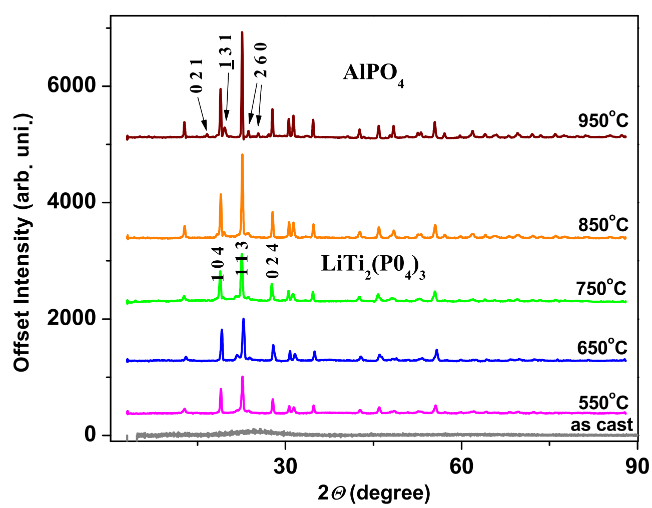

Fig. 1 XRD patterns of glass–ceramic samples. Diffraction pattern, for the as-cast glass, is included for comparison

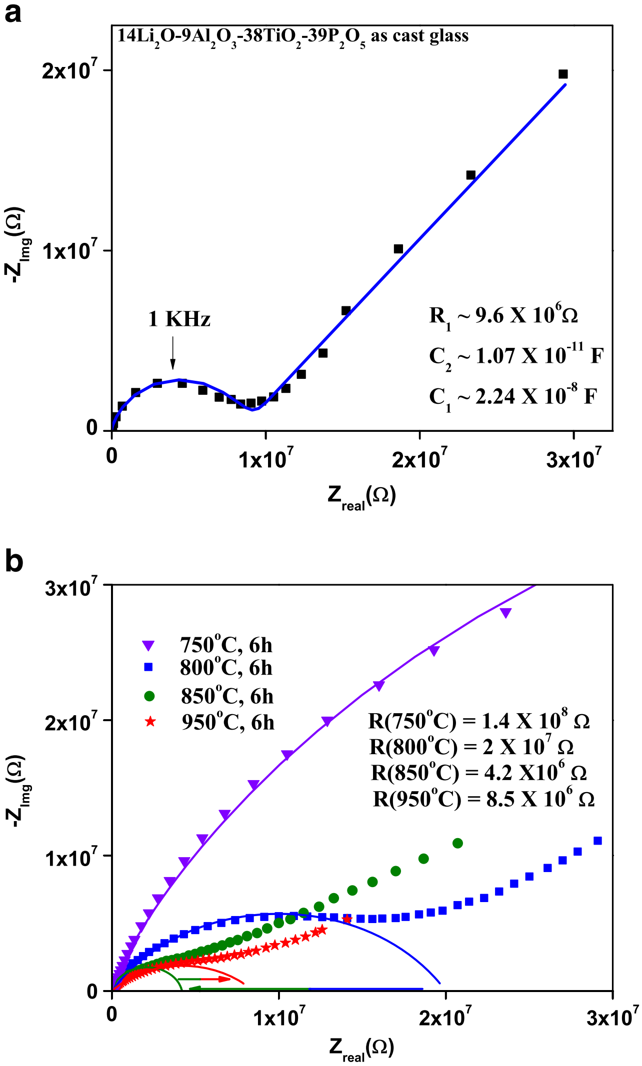

Fig. 2 **a** Impedance plot of as-cast LATP glass with semicircular fit and corresponding equivalent RC values are given in the figure. **b** Impedance plots of glass–ceramic samples heat-treated at different temperatures. Semicircular fits corresponding to equivalent *RC* circuits are also shown. Fitted values of *R* are listed for comparison

from the relation $\omega=1/RC$. The values were $R_1=9.6\times10^6\,\Omega$ and $C_2=1.07\times10^{-11}$ F. These values were indicative of Li ion conduction through the bulk of the glass. The low-frequency "spike" represented charge built-up at the blocking metal electrode (with $C_1=2.24\times10^{-8}$ F), suggesting impedance barrier to charge transfer between metal electrode and glass sample. It also implied that the conduction is ionic in nature.

Figure 2b is an impedance plot of some of the glass–ceramic samples heat-treated at different temperatures shown together for comparison. Only the high frequency segment of the curvature data is visible for samples heat-treated at 750 °C. Semicircular fits corresponding to equivalent *RC* circuits are also shown along with data points for these samples. It is interesting to observe that the value of *R* decreased with heat treatment temperature up to 850 °C. This trend reversed for samples heat-treated above 850 °C.

The frequency dependence of conductivity obeyed Johnscher's power law $\sigma_{ac}=\sigma_{dc}+Af^n$ (as shown in Fig. 3), where *A* is a constant and *n* is the frequency exponent. The value of *n* is in a range of $0\leq n\leq1$. Curves corresponding to different measurement temperatures were plotted together. For each measurement temperature, dc conductivity was calculated by fitting data to above power law. Fitted values were in good agreement with the values obtained from corresponding impedance plots (where the semicircle intercepts the real axis).

Figure 4 shows the temperature variation of dc conductivity for the entire sample series. DC conductivity obeys Arrhenius equation $\sigma_{dc}=A\ \exp\ (-E_a/kT)$ where *T* is the absolute temperature, *A* is pre-exponential factor, E_a is the activation energy for conduction, and *k* is the gas constant. For each sample, activation energy was calculated by fitting data to the Arrhenius equation above.

Its trend with heat treatment temperature is shown in Fig. 5. As-cast sample showed 0.65 eV, while for the highest conducting sample it was 0.325 eV. For samples heat-treated above 850 °C, it increased to 0.76 eV.

The inset of Fig. 4 shows samples heat-treated at 550 °C for different time durations. Only a slight change in conductivity was observed when heat treatment duration was increased by a factor of 2 or more. This suggested that at a given temperature no significant change in morphology or phase content occurred with increase in time duration. It also implied conductivity being independent of these parameters. Therefore, it was decided to heat-treat other samples only for 6 h each at different temperatures.

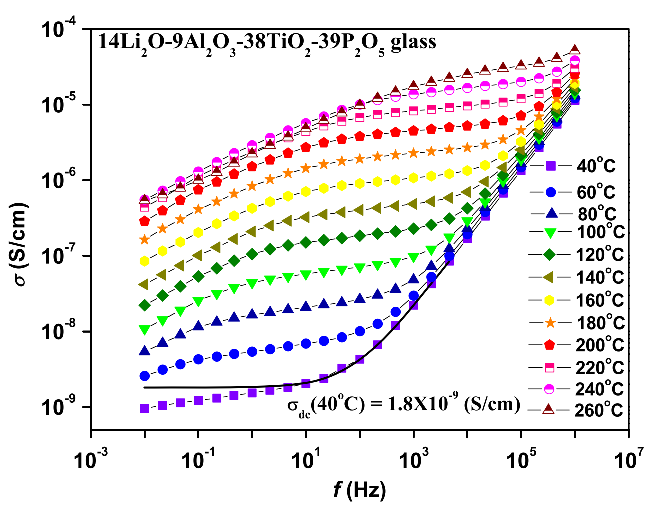

Fig. 3 Conductivity versus frequency response of as-cast glass over temperature range 40–260 °C. The *black line* is Johnscher's power law fit to the data curve recorded at 40 °C

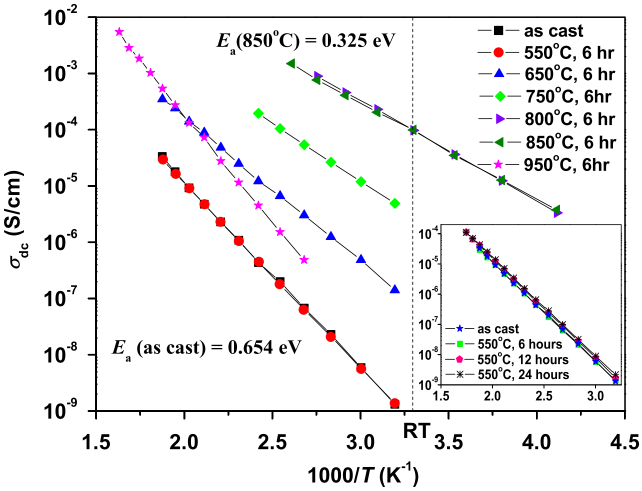

Fig. 4 Arrhenius plot of dc conductivity versus inverse temperature for the samples heat-treated for 6 h at different temperatures. Data on as-cast glass is included for comparison. *Inset* shows dc conductivity versus inverse temperature for samples heat-treated at 550 °C for different time durations

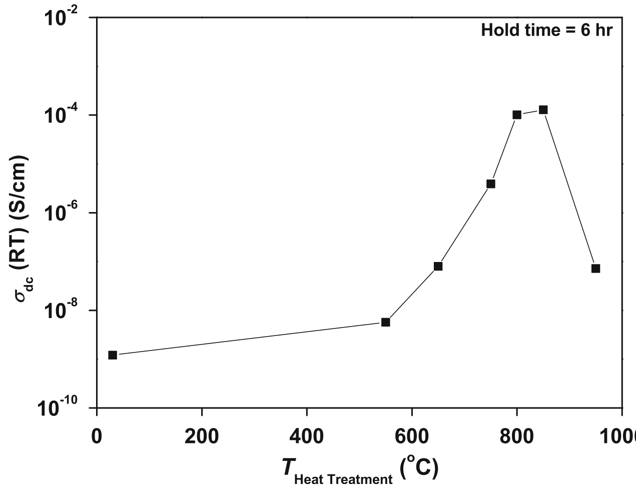

Fig. 6 Room temperature dc conductivity plotted against heat treatment temperature for the glass–ceramic series samples

Variation of dc conductivity measured at room temperature for LATP glass and glass–ceramic is depicted in Fig. 6. DC conductivity (measured at room temperature) increased rapidly with heat treatment temperature up to 850 °C. Maximum room temperature dc conductivity of the order of 10^{-4} S/cm was obtained for the sample heat-treated at 850 °C. Further increase in heat treatment temperature resulted in decreased conductivity. A similar trend in conductivity was reported [10]. Such conductivity behavior can be understood with the help of XRD data. $LiTi_2(PO_4)_3$ phase was present in all heat-treated samples. As the heat treatment temperature increased up to 850 °C, XRD peak intensity corresponding to $LiTi_2(PO_4)_3$ phase also increased. Therefore, $LiTi_2(PO_4)_3$ phase is mainly responsible for enhanced conductivity. Above 850 °C, a second crystalline phase, namely, $AlPO_4$, was formed. $AlPO_4$ phase grew in samples heat-treated at 900 °C and beyond. Insulating nature of $AlPO_4$ phase dominated the overall behavior in these samples (already containing $LiTi_2(PO_4)_3$ phase), resulting in decreased conductivity.

Relative crystalline phase contents of the glass–ceramic samples were calculated using XRD plots. It was assumed that XRD measurement parameters remain the same for all samples. Considering 0% crystalline phase contents in as-cast glass sample and 100% crystalline phase contents for fully ceramic phase, relative crystalline content values were estimated with respect to maximum peak intensity of the prominent peak observed ~24 (2Θ) position corresponding to $LiTi_2(PO_4)_3$ phase. As shown in Fig. 7, room temperature dc conductivity started to increase at about 30% crystalline content and attained maximum between 40% and 65%. It is important to emphasize that the accuracy of

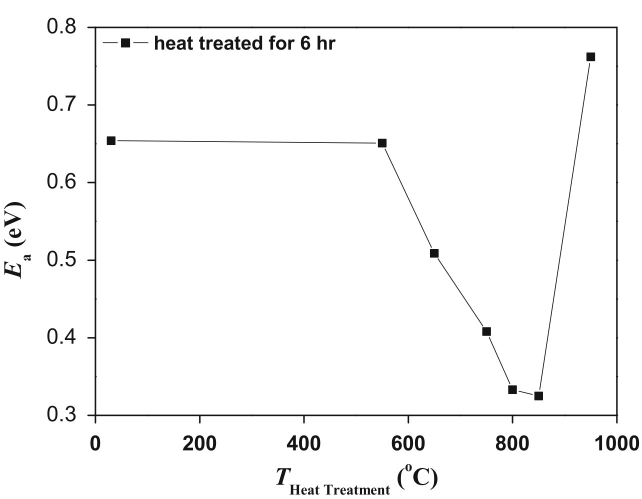

Fig. 5 Variation of activation energy for conduction with heat treatment temperature

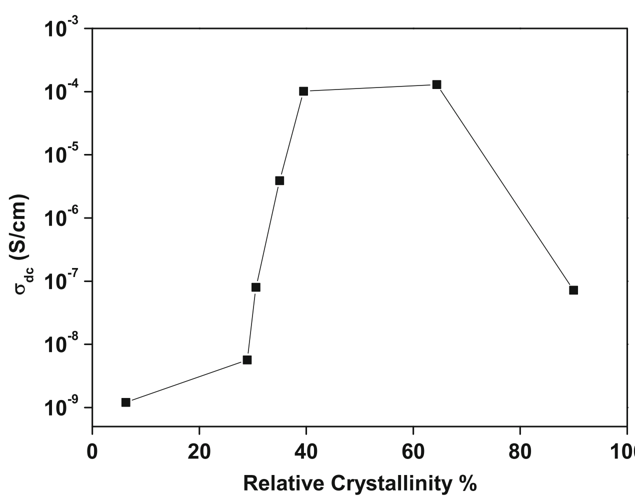

Fig. 7 Room temperature dc conductivity versus relative crystalline contents

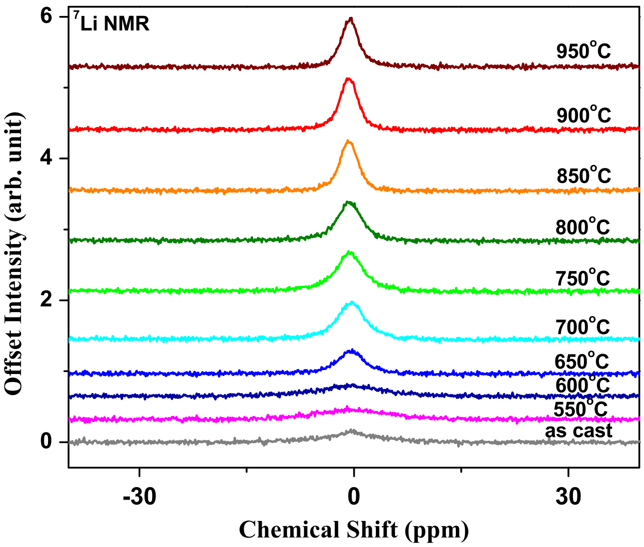

Fig. 8 ^{7}Li NMR spectra of glass–ceramic system plotted together for easy comparison

this estimate is lesser for samples heat-treated above 850 °C. As explained earlier, above this temperature $AlPO_4$ phase started to grow. Therefore, the total crystalline phase content of these samples would consist of contribution from $LiTi_2(PO_4)_3$ phase as well as $AlPO_4$ phase.

NMR measurements

^{7}Li NMR spectra of this glass–ceramic system are shown in Fig. 8 as a function of heat treatment temperature. The central transition indicated the presence of mobile ^{7}Li ions in the entire sample series. The line width of ^{7}Li static NMR spectra is inversely proportional to the jump rate of Li ions in the material (motional narrowing effect). Samples annealed

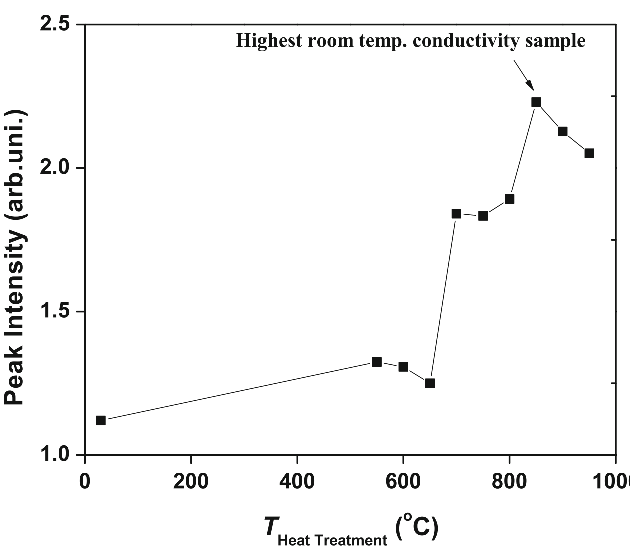

Fig. 9 Peak intensity of ^{7}Li static NMR spectra versus heat treatment temperature

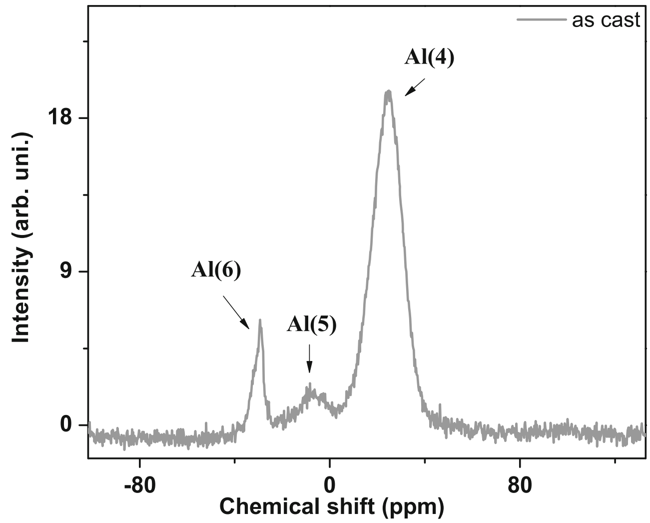

Fig. 10 ^{27}Al MAS NMR spectrum of as cast glass

below second crystallization temperature (i.e., <650 °C) showed broader spectra. As the annealing temperature was increased above 650 °C, spectral width decreased, indicating increased mobility of Li ions.

It was also observed that for the sample with highest room temperature conductivity, i.e., heat-treated at 850 °C, ^{7}Li NMR peak intensity was also maximum as seen in Fig. 9.

The activation energy for conduction decreased with increasing heat treatment temperature up to 850 °C (as shown in Fig. 5), suggesting that the presence of LTO structure enabled easier passages for ^{7}Li ion movement. Similar observations were reported in pellet pressed and sintered samples of $Li_{1.3}Al_{0.3}Ti_{1.7}(PO_4)_3$ [14].

Figure 10 shows ^{27}Al NMR recorded on as cast glass sample. Three distinct peaks were observed at approximately −29, −8, and 25 ppm. The peaks at −29 and 25 ppm

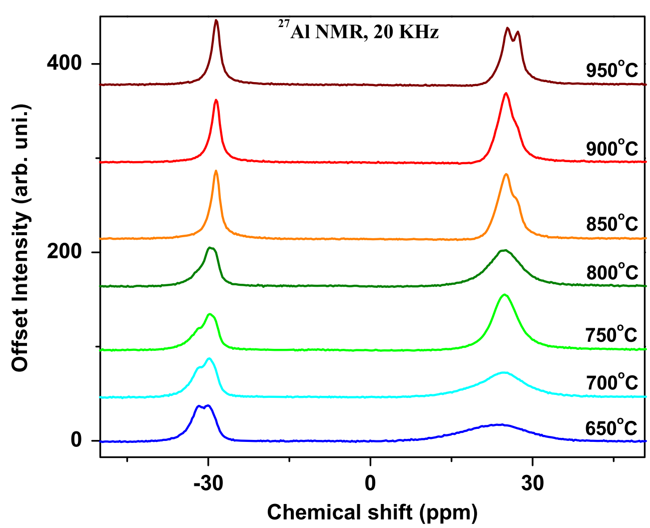

Fig. 11 ^{27}Al MAS NMR spectra for samples heat treated from 650 °C to 950 °C

were identified as positions for octahedral and tetrahedral coordinated Al–O units. The octahedral coordinated peak was shifted to lower part in ppm as compared to αAl_2O_3, indicating greater electronegativity of P^{+5} and better shielding of six coordinated Al in this glass structure. The peak at −8 ppm was interpreted as five coordinated Al sites corresponding to an amorphous phase. Similar three peak positions were also reported earlier in polycrystalline samples of $Li_{1.3}Al_{0.3}Ti_{1.7}(PO_4)_3$ [9, 13, 14].

The evolution of these three peaks with heat treatment temperature was also recorded in our sample series as shown in Fig. 11. The five coordinated peaks persisted in samples heat-treated up to 800 °C, although its intensity was far lesser compared to octahedral and tetrahedral coordination peaks, suggesting the presence of underlying glassy matrix. (The presence of amorphous phase could not be detected in XRD spectra for its far lesser intensity.) For samples heat-treated in the range 650–800 °C, two closely associated peaks were observed, indicating highly localized distortion at six coordinated Al sites. However, for samples heat-treated at 850 °C and above (when $AlPO_4$ phase could be detected in XRD), the tetrahedral site showed such bond distortion. No systematic trend was observed (figure not shown here) in the ratio of octahedral- to tetrahedral-substituted Al with heat treatment temperature.

The asymmetry and broadening of the ^{31}P peak (figure not shown here) suggested a distribution of multiple phosphorous sites as reported earlier in a polycrystalline sample of $Li_{1.3}Al_{0.3}Ti_{1.7}(PO_4)_3$ [14].

Based on the observations above, attempts are being made to optimize this glass–ceramic further. One way is to avoid the formation of insulating $AlPO_4$ phase at higher temperatures by partially substituting Al with Ge/Ti, etc. [11, 12]. Another approach is to control the growth of $LiTi_2(PO_4)_3$ phase by tuning heat treatment temperatures and time duration to optimize conductivity.

Conclusion

LATP glass was fabricated by conventional melt quenching technique. This glass was heat-treated at different temperatures in the range 550–950 °C, resulting in a dense glass–ceramic material with varying percentages of ceramic contents. LTP was found to be the dominant crystalline phase contributing to the enhanced conductivity. The highest room temperature dc ionic conductivity was found to be of the order of 10^{-4} S/cm for samples crystallized at 850 °C. NMR characterization confirmed the presence of mobile $^7Li^+$ ions and also revealed the presence of glassy matrix in samples heat-treated up to 800 °C. The optimized glass–ceramic material is being used in pulse laser deposition to fabricate thin film electrolyte. The results would be reported separately.

Acknowledgement The authors acknowledge Department of Science and Technology, Govt. of India (DST)–Japanese Science and Technology (JST) collaborative program. The authors thank Indian Institute of Technology Bombay and Tohoku University for infrastructural support. SS thanks DST for financial support.

References

1. Kawamura J, Kuwata N, Toribami K, Sata N, Kamishima O, Hattori T (2004) Solid State Ionics 175:273–276
2. Kuwata N, Kawamura J, Toribami K, Hattori T, Sata N (2004) Electrochem Commun 6:417–421
3. Brazier A, Dupont L, Laffont LD, Kuwata N, Kawamura J, Tarascon JM (2008) Chem Mater 20:2352–2359
4. Kuwata N, Iwagami N, Kawamura J (2009) Solid State Ionics 180:644–648
5. Kuwano J, Sato N, Kato M, Takano K (1994) Solid State Ionics 70(71):332–336
6. Aono H, Sugimoto E, Sadaoka Y, Imanaka N, Adachi G (1990) J Electrochem Soc 137:1023–1027
7. Aono H, Sugimoto E, Sadaoka Y, Imanaka N, Adachi G (1989) J Electrochem Soc 136:590–591
8. Wong S, Newman PJ, Best AS, Nairn KM, MacFarlane DR, Forsyth M (1998) J Mater Chem 8:2199–2203
9. Best AS, Forsyth M, MacFarlane DR (2000) Solid State Ionics 136:339–344
10. Fu J (1997) Solid State Ionics 96:195–200
11. Fu J (1997) Solid State Ionics 104:191–194
12. Chowdari BVR, Subba Rao GV, Lee GYH (2000) Solid State Ionics 136–137:1067–1075
13. Forsyth M, Wong S, Nairn KM, Best AS, Newman PJ, MacFarlane DR (1999) Solid State Ionics 124:213–219
14. Nairn KM, Forsyth M, Greville M, MacFarlane DR, Smith ME (1996) Solid State Ionics 86–88:1397–1402